Optical binding and lateral forces on chiral particles in linearly polarized plane waves

Hongsheng Shi [1], Hongxia Zheng,[2] Huajin Chen [1,2,*] Wanli Lu,[3,†] Shiyang Liu,[4] and Zhifang Lin[2,5]

[1]*School of Electrical and Information Engineering, Guangxi University of Science and Technology, Liuzhou, Guangxi 545006, China*

[2]*State Key Laboratory of Surface Physics (SKLSP) and Department of Physics, Fudan University, Shanghai 200433, China*

[3]*School of Physics, China University of Mining and Technology, Xuzhou, Jiangsu 221116, China*

[4]*Institute of Information Optics, Zhejiang Normal University, Jinhua, Zhejiang 321004, China*

[5]*Collaborative Innovation Center of Advanced Microstructures, Nanjing University, Nanjing 210093, China*

(Received 30 December 2019; revised manuscript received 25 February 2020; accepted 10 March 2020; published 7 April 2020)

We demonstrate numerically and analytically the optical binding between a pair of chiral nanoparticles immersed in a plane wave of linear polarization. The numerical results based on the full wave simulation show that, when the electric field of the incident wave is polarized along the pair axis (the line connecting the particle pair), the closest dimer can be formed at particle separation around 1.25λ, with λ denoting the incident wavelength, while when the electric field is polarized normal to the pair axis, the nearest dimer is formed with a separation of one wavelength. In both cases, there exist multiple stable dimer states due to the spatially oscillatory decaying behavior of the binding force with the increase of particle distance. Interestingly, there also appears a lateral optical force exerted on each particle in the direction normal to both the pair axis and light flow, when either or both particles have chirality. Analytical analysis within the dipole approximation indicates that the binding force comes dominantly from the gradient of the optical potential, irrespective of particle chirality. The lateral force, on the other hand, has multiple origins. In addition to the gradient force, the radiation force, the curl force, and the spin force may make significant contributions dependent on the particle chirality, as the particles approach each other.

DOI: 10.1103/PhysRevA.101.043808

I. INTRODUCTION

Optical binding (OB) [1,2] describes an intriguing phenomenon where a light-mediated interparticle interaction can induce self-organization of microscopic particles and is thus distinct fundamentally from the optical trapping due to the intensity gradient of incident light [3]. Since first proposed by Burns *et al.*, OB has attracted growing interest and has been extensively studied in a diversity of materials, such as dielectric particles [4,5], metallic nanoparticles [6], magnetodielectric particles [7], colloidal particles [8], birefringent particles [9], and many others [10–12]. In contrast, much less attention has been dedicated to chiral particles due to the computational complexity [3,13,14]. However, chirality widely exists in living matter and nature and plays a key role in physics, biology, chemistry, pharmaceuticals, and so on, due to the fact that it can provide a lot of new opportunities to fundamental research and practical applications in optical manipulations.

On the other hand, significant research in OB focuses on the binding force along the axis of two or more particles that is either perpendicular or parallel to light propagation [1–6,8–17], whereas in the direction perpendicular to both the pair axis and the light propagation where there is neither energy flow nor an intensity gradient of incident light, a new lateral optical force [18,19] may be exerted on the particles, but it is less considered. Only two exceptions show the existence of the lateral force on the two particles consisting of one dielectric particle and one magnetodielectric particle [7] and a pair of chiral particles with opposite handiness [20]. The lateral force has become an intriguing focus of study in recent years [21–32] and could give rise to some novel phenomena and potential applications in OB.

In this paper, we investigate the OB and lateral optical forces of a pair of particles with different chirality parameters under the illumination of a plane wave with two different linear polarizations either parallel or normal to the pair axis (i.e., the line connecting the particle pair). Based on the full wave simulation (FWS), we calculate the transverse optical force, perpendicular to the direction of light propagation, acting on each particle as a function of the interparticle separation. For the paired particles illuminated by the plane wave of the same polarization, the binding forces exhibit a similar behavior for the two particles of different combinations, irrespective of the particle chirality. However, the switch of the linear polarization from on-axis direction (parallel to the pair axis) to its orthogonal direction (normal to the pair axis) will substantially change the binding force on both the magnitude and the evolution behavior with respect to the particle separation. There also exist multiple stable dimer states with different interparticle separations, and the closest dimer can be formed at the particle distance separated by around λ or 1.25λ for the two different linear polarizations. Meanwhile, it is demonstrated that, when either one or both particles are

*huajinchen13@fudan.edu.cn

†luwl@cumt.edu.cn

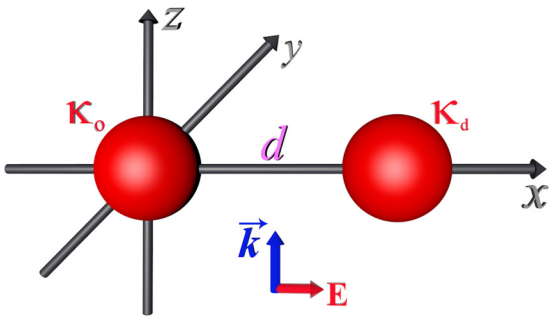

FIG. 1. Sketch of a pair of spherical particles with different chirality illuminated by a linearly polarized plane wave propagating along the z direction. The parameters κ_o and κ_d denote the chirality parameters of two particles located at the origin and $x = d$, respectively. The two particles have the radius $r_s = 0.1$ μm, the permittivity $\varepsilon_s = 2.5$, and the permeability $\mu_s = 1.0$. The incident wavelength is $\lambda = 1.064$ μm.

chiral, the particle chirality can induce a lateral optical force on each particle in the direction perpendicular to the pair axis and the illuminating direction. Analytical results based on the dipole approximation show that the binding force is dominated by the gradient force while the lateral force comes from the simultaneous contribution of the gradient force, the radiation force, the curl force, as well as the spin force. Our results could be used in chiral discrimination and particle self-assembly such as biological cells and chiral molecules.

II. OPTICAL FORCE FROM FULL WAVE SIMULATION

For simplicity, we consider a pair of spherical particles wherein one sphere is fixed at the origin and the other sphere at $x = d$ illuminated by a plane wave propagating along the z axis, as sketched in Fig. 1. Here we assume the two particles have a radius $r_s = 0.1$ μm and the incident wavelength $\lambda = 1.064$ μm throughout the paper. For a chiral medium, the constitutive relations are described by [33–35]

$$\mathbf{D} = \varepsilon_0\varepsilon_s\mathbf{E} + i\kappa\sqrt{\varepsilon_0\mu_0}\,\mathbf{H}, \quad \mathbf{B} = \mu_0\mu_s\mathbf{H} - i\kappa\sqrt{\varepsilon_0\mu_0}\,\mathbf{E}, \tag{1}$$

where ε_0 and μ_0 are the permittivity and permeability in vacuum, and ε_s and μ_s are the relative permittivity and permeability of the chiral material, respectively. κ is the chirality parameter and meets the relation $\kappa^2 < \varepsilon_s\mu_s$ [35]. The planar eigenmodes for a plane wave in chiral media are $k_1 = k_0(\sqrt{\varepsilon_s\mu_s} + \kappa)$ and $k_2 = k_0(\sqrt{\varepsilon_s\mu_s} - \kappa)$, corresponding to two circularly polarized states of light, and k_0 represents the wave number in vacuum.

In our computational model, the numerical calculation of optical force on spherical particles can be performed based on the FWS approach to very high precision. First, we solve the fields hitting on either particle using the FWS approach based on multiple-scattering theory [5,33,36] and the generalized Lorenz-Mie theory [37]. The fields $\mathbf{E}$ and $\mathbf{H}$ acting on sphere j consist of the initial incident field and the scattered fields from the other sphere, and thus can be written in terms of the vector spherical wave functions $\mathbf{M}_{mn}^{(J)}$ and $\mathbf{N}_{mn}^{(J)}$ [5,36]

$$\begin{aligned}\mathbf{E} &= \sum_{n,m} iE_{mn}\big[a_{mn}\mathbf{N}_{mn}^{(3)}(k,\mathbf{r}) + b_{mn}\mathbf{M}_{mn}^{(3)}(k,\mathbf{r}) \\ &\quad - p_{mn}\mathbf{N}_{mn}^{(1)}(k,\mathbf{r}) - q_{mn}\mathbf{M}_{mn}^{(1)}(k,\mathbf{r})\big], \\ \mathbf{H} &= \frac{k}{\omega\mu}\sum_{n,m} E_{mn}\big[b_{mn}\mathbf{N}_{mn}^{(3)}(k,\mathbf{r}) + a_{mn}\mathbf{M}_{mn}^{(3)}(k,\mathbf{r}) \\ &\quad - q_{mn}\mathbf{N}_{mn}^{(1)}(k,\mathbf{r}) - p_{mn}\mathbf{M}_{mn}^{(1)}(k,\mathbf{r})\big],\end{aligned} \tag{2}$$

with

$$E_{mn} = |E_0|i^n C_{mn}, \quad C_{mn} = \left[\frac{(2n+1)}{n(n+1)}\frac{(n-m)!}{(n+m)!}\right]^{\frac{1}{2}}.$$

In Eqs. (2), k is the wave number in the background medium, ε and μ are the permittivity and permeability in the background medium, and ω is the circular frequency. The a_{mn} and b_{mn} are scattering coefficients of sphere j, which are given by

$$a_{mn} = a_n^{(1)}p_{mn} + a_n^{(2)}q_{mn}, \quad b_{mn} = b_n^{(1)}q_{mn} + b_n^{(2)}p_{mn}. \tag{3}$$

In Eq. (3), p_{mn} and q_{mn} denote the expansion coefficients of the fields acting on sphere j, and read [5,36]

$$\begin{aligned}p_{mn} &= p_{mn}^{(j,j)} - \sum_{l\neq j}\sum_{v,u}\big[a_{uv}^{(l)}A_{mn}^{uv}(l,j) + b_{uv}^{(l)}B_{mn}^{uv}(l,j)\big], \\ q_{mn} &= q_{mn}^{(j,j)} - \sum_{l\neq j}\sum_{v,u}\big[a_{uv}^{(l)}B_{mn}^{uv}(l,j) + b_{uv}^{(l)}A_{mn}^{uv}(l,j)\big],\end{aligned} \tag{4}$$

where $A_{mn}^{uv}(l,j)$ and $B_{mn}^{uv}(l,j)$ are the translation coefficients given in Ref. [5]. The Mie coefficients $a_n^{(1)}$, $a_n^{(2)}$, $b_n^{(1)}$, and $b_n^{(2)}$ for chiral spheres can be written as [33,38]

$$\begin{aligned}a_n^{(1)} &= \big[A_n^{(2)}V_n^{(1)} + A_n^{(1)}V_n^{(2)}\big]Q_n, \\ a_n^{(2)} &= \big[A_n^{(1)}W_n^{(2)} - A_n^{(2)}W_n^{(1)}\big]Q_n, \\ b_n^{(1)} &= \big[B_n^{(1)}W_n^{(2)} + B_n^{(2)}W_n^{(1)}\big]Q_n, \\ b_n^{(2)} &= a_n^{(2)},\end{aligned} \tag{5}$$

with

$$\begin{aligned}A_n^{(i)} &= Z_sD_n^{(1)}(x_i) - D_n^{(1)}(x_0), \\ B_n^{(i)} &= D_n^{(1)}(x_i) - Z_sD_n^{(1)}(x_0), \\ W_n^{(i)} &= Z_sD_n^{(1)}(x_i) - D_n^{(3)}(x_0), \\ V_n^{(i)} &= D_n^{(1)}(x_i) - Z_sD_n^{(3)}(x_0), \\ Q_n &= \frac{\psi_n(x_0)/\xi_n(x_0)}{V_n^{(1)}W_n^{(2)} + V_n^{(2)}W_n^{(1)}}.\end{aligned}$$

Here $x_0 = k_0r_s$, $x_1 = k_1r_s$, and $x_2 = k_2r_s$. $Z_s = \sqrt{\mu_s/\varepsilon_s}$ is the wave impedance of the particle, $\psi_n(x)$ and $\xi_n(x)$ are, respectively, the Riccati-Bessel functions of the first and third kinds, while $D_n^{(1)}(x) = \psi_n'(x)/\psi_n(x)$ and $D_n^{(3)}(x) = \xi_n'(x)/\xi_n(x)$ are the corresponding logarithmic derivatives. Note that α_{em} vanishes for a nonchiral particle ($\kappa = 0$).

Then the time-averaged optical force acting on a spherical particle can be exactly calculated by a surface integral of the time-averaged Maxwell stress tensor over the particle surface

[39,40]

$$\langle \mathbf{F} \rangle = \oint_S \hat{\mathbf{r}} \cdot \langle \overleftrightarrow{\mathbf{T}} \rangle dS, \tag{6}$$

where $\hat{\mathbf{r}}$ is related to the outward unit normal on the surface S, and the time-averaged Maxwell stress tensor is given by [39]

$$\langle \overleftrightarrow{\mathbf{T}} \rangle = \tfrac{1}{2}\mathrm{Re}\big[\varepsilon \mathbf{E}\mathbf{E}^* + \mu \mathbf{H}\mathbf{H}^* - \tfrac{1}{2}(\varepsilon \mathbf{E}\cdot\mathbf{E}^* + \mu \mathbf{H}\cdot\mathbf{H}^*)\overleftrightarrow{\mathbf{I}}\big]. \tag{7}$$

In Eq. (7), the superscript * represents the complex conjugate, and the $\overleftrightarrow{\mathbf{I}}$ denotes the unit dyad.

For a chiral sphere immersed in the lossless background medium, the integral in Eq. (6) can be performed at infinity due to the conservation of momentum. After some complex mathematical manipulations, the expressions of optical force can eventually be simplified to [41–43]

$$F_x = \mathrm{Re}[F_1], \quad F_y = \mathrm{Im}[F_1], \quad F_z = \mathrm{Re}[F_2]. \tag{8}$$

In Eqs. (8), the complex functions F_1 and F_2 can be expressed as

$$F_1 = \frac{2\pi\varepsilon E_0^2}{k^2}\sum_{n,m}\big[c_{11}F_1^{(1)} - c_{12}F_1^{(2)} + c_{13}F_1^{(3)}\big],$$
$$F_2 = -\frac{4\pi\varepsilon E_0^2}{k^2}\sum_{n,m}\big[c_{21}F_2^{(1)} + c_{22}F_2^{(2)}\big], \tag{9}$$

with the coefficients

$$c_{11} = \left[\frac{(n-m)(n+m+1)}{n^2(n+1)^2}\right]^{\frac{1}{2}},$$
$$c_{12} = \left[\frac{n(n+2)(n+m+1)(n+m+2)}{(n+1)^2(2n+1)(2n+3)}\right]^{\frac{1}{2}},$$
$$c_{13} = \left[\frac{n(n+2)(n-m)(n-m+1)}{(n+1)^2(2n+1)(2n+3)}\right]^{\frac{1}{2}},$$
$$c_{21} = \left[\frac{n(n+2)(n-m+1)(n+m+1)}{(n+1)^2(2n+1)(2n+3)}\right]^{\frac{1}{2}},$$
$$c_{22} = \frac{m}{n(n+1)},$$

and

$$F_1^{(1)} = \tilde{a}_{mn}\tilde{b}^*_{m_1 n} + \tilde{b}_{mn}\tilde{a}^*_{m_1 n} - \tilde{p}_{mn}\tilde{q}^*_{m_1 n} - \tilde{q}_{mn}\tilde{p}^*_{m_1 n},$$
$$F_1^{(2)} = \tilde{a}_{mn}\tilde{a}^*_{m_1 n_1} + \tilde{b}_{mn}\tilde{b}^*_{m_1 n_1} - \tilde{p}_{mn}\tilde{p}^*_{m_1 n_1} - \tilde{q}_{mn}\tilde{q}^*_{m_1 n_1},$$
$$F_1^{(3)} = \tilde{a}_{mn_1}\tilde{a}^*_{m_1 n} + \tilde{b}_{mn_1}\tilde{b}^*_{m_1 n} - \tilde{p}_{mn_1}\tilde{p}^*_{m_1 n} - \tilde{q}_{mn_1}\tilde{q}^*_{m_1 n},$$
$$F_2^{(1)} = \tilde{a}_{mn}\tilde{a}^*_{mn_1} + \tilde{b}_{mn}\tilde{b}^*_{mn_1} - \tilde{p}_{mn}\tilde{p}^*_{mn_1} - \tilde{q}_{mn}\tilde{q}^*_{mn_1},$$
$$F_2^{(2)} = \tilde{a}_{mn}\tilde{b}^*_{mn} - \tilde{p}_{mn}\tilde{q}^*_{mn},$$

where $m_1 = m+1$, $n_1 = n+1$, and the coefficients

$$\tilde{a}_{mn} = a_{mn} - \tfrac{1}{2}p_{mn}, \quad \tilde{p}_{mn} = \tfrac{1}{2}p_{mn},$$
$$\tilde{b}_{mn} = b_{mn} - \tfrac{1}{2}q_{mn}, \quad \tilde{q}_{mn} = \tfrac{1}{2}q_{mn}. \tag{10}$$

Next, we use the FWS approach to calculate the two components of the transverse force F_x (binding force) and F_y (lateral force) on a pair of particles with different combinations of particle chirality, namely, two nonchiral particles, one nonchiral particle and one chiral particle, two chiral particles with the same handedness, and two chiral particles with the opposite handedness, under the illumination of a linearly polarized plane wave. The results are presented in Fig. 2, where the incident electric field is polarized along the x axis and all the other parameters are the same as in Fig. 1. One can see from Figs. 2(a) and 2(b) that the binding force F_x on each particle for different cases have nearly same magnitudes, and thus it is insensitive to the particle chirality. Also, for the aforementioned four types of combinations, F_x exhibits a similar behavior in that the nearest dimer can be formed at a separation about 1.25λ and there also appears multiple stable dimer states, with the magnitudes of F_x decreased with the particle distance, as illuminated by the enlarged views in Figs. 2(e) and 2(f). Nonetheless, for the lateral force F_y the situation is dramatically different for case 1 with two nonchiral particles ($\kappa_o = \kappa_d = 0$) and the chiral cases when either or both particles have the chirality, as shown in Figs. 2(c) and 2(d), where the vanishing lateral force F_y in case 1 comes into appearance on each particle and shows different phenomena for different chiral cases. Concretely, for the case 2 ($\kappa_o = 0$, $\kappa_d = 0.5$), the lateral forces F_y exerted on the two particles have the same directions but different magnitudes in the range $d < 0.7$ μm, where the magnitude of F_y on the nonchiral particle is relatively smaller than that acting on the chiral particle. In case 3 ($\kappa_o = \kappa_d = 0.5$), the lateral forces F_y exerted on the two chiral particles have always the same magnitudes but opposite signs. As a result, the lateral force

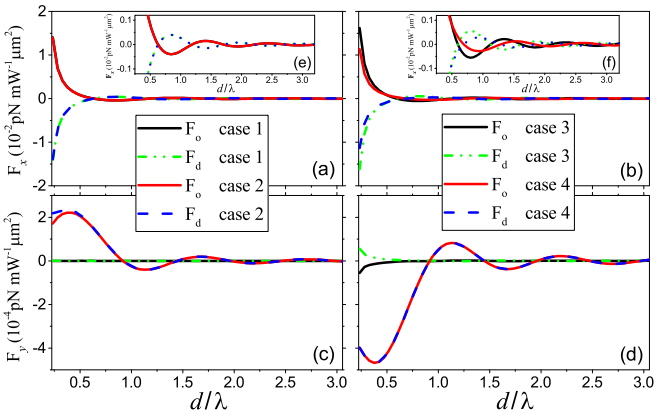

FIG. 2. The transverse optical force acting on a pair of particles versus the separation d between the chiral particles immersed in a plane wave with its electric field polarized along the x axis. The (a), (b) binding force F_x and (c), (d) the lateral optical force F_y are calculated for the paired particles of four different combinations of particle chirality. F_o (solid lines) and F_d (dashed lines) denote the optical force exerted on the particle located at the origin and $x = d$, respectively. The two particles in case 1 with two nonchiral particles ($\kappa_o = \kappa_d = 0$) and case 2 with one nonchiral particle and one chiral particle ($\kappa_o = 0$, $\kappa_d = 0.5$) correspond to panels (a) and (c); case 3 with two chiral particles of the same handedness ($\kappa_o = \kappa_d = 0.5$) and case 4 with two chiral particles of the opposite handedness ($\kappa_o = -\kappa_d = 0.5$) correspond to panels (b) and (d). Panels (e) and (f) are enlarged views of panels (a) and (b), respectively.

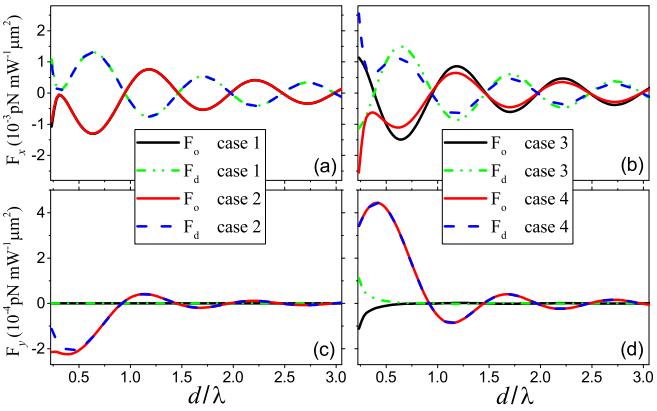

FIG. 3. Same as Fig. 2, except that the plane wave with its electric field polarized along y axis is considered here.

may rotate the two particles around their center of mass. For the case 4 ($\kappa_o = -\kappa_d = 0.5$), the identical lateral force F_y emerges on each particle and thereby can push the two particles in the lateral direction simultaneously. The similar result is also investigated in our previous work [20]. Our results could be used to discriminate paired molecules with different chirality [44,45]. In addition, all the lateral forces for the chiral cases show an oscillatory behavior with a period of about the incident wavelength λ as a consequence of the field retardation from the multiple scattering between the two particles.

To further examine the polarization dependence of the forces F_x and F_y on the paired particles, the incident plane wave with the electric field polarized along the y axis is also considered. The results are presented in Fig. 3, where all the binding forces F_x corresponding to the same four cases in Fig. 2 have a much smaller magnitude in the small interparticle separation as compared with the illumination by the x-polarized plane wave and an oscillation behavior can also be observed. In particular, there also exist multiple stable dimer states separated by multiples of wavelengths and the closest dimer is formed with a separation of around one wavelength; see Figs. 3(a) and 3(b). In addition, by further examining Fig. 2(a) it can be found that the binding force F_x in case 2 is nearly the same as that in case 1 with two nonchiral particles, while in cases 3 and 4 it exhibits an evident difference. By comparing Fig. 2 with Fig. 3, it can be found that the lateral forces F_y for cases 2 and 4 have the same magnitudes but opposite signs due to the change in the incident polarization, suggesting an additional degree of freedom for the optical manipulation by the polarization of light.

Finally, note that there is no lateral force when a single chiral particle is illuminated by a plane wave. In the proximity of a conventional particle, however, a lateral force acting on the chiral particle will be induced, even though the incident wave does not apparently break the symmetry in lateral directions. This is shown by the blue dashed line in Fig. 3(c). By increasing the radius of the nearby conventional particle while keeping the fringe-to-fringe separation between particles unchanged, one will reproduce the lateral optical force on chiral particles near a surface [19] from the configuration shown in Fig. 1. The physics of the lateral force lies actually in the fact that the symmetry of optical fields in which the particle is immersed is broken in the presence of the nearby surface or particle, due to multiple scattering between the chiral and nonchiral scatterers, although the incident fields apparently stay symmetric with respect to $\pm y$. Most lateral forces originate indeed from this type of symmetry breaking of the ambient fields impinging on the particle.

III. OPTICAL FORCE FROM THE DIPOLE APPROXIMATION

To trace the physical origin of the transverse force, the analytical expressions of the optical force acting on a chiral particle can be obtained within the dipole approximation due to the particle size being much smaller than the incident wavelength. Thus, the time-averaged optical force on a chiral particle can be expressed in terms of the electric- and magnetic-dipole moments [19,20,32,46–49]

$$\langle \mathbf{F} \rangle = \frac{1}{2}\mathrm{Re}\left[(\nabla \otimes \mathbf{E}^*)\cdot \mathbf{p} + (\nabla \otimes \mathbf{B}^*)\cdot \mathbf{m} - \frac{k^4}{6\pi\varepsilon c}(\mathbf{p}\times \mathbf{m}^*)\right], \tag{11}$$

where c is the velocity of light in vacuum, the symbol $\otimes$ denotes the dyadic product, and $\mathbf{E}$ and $\mathbf{B}$ are the fields exerted on the particle. The electric- and magnetic-dipole moments can be written as [19,20,48,50,51]

$$\mathbf{p} = \alpha_{ee}\mathbf{E} + \alpha_{em}\mathbf{B}, \quad \mathbf{m} = -\alpha_{em}\mathbf{E} + \alpha_{mm}\mathbf{B}, \tag{12}$$

with the polarizabilities

$$\alpha_{ee} = \frac{i6\pi\varepsilon}{k^3}a_1^{(1)}, \quad \alpha_{mm} = \frac{i6\pi}{\mu k^3}b_1^{(1)}, \quad \alpha_{em} = -\frac{6\pi}{Z_b k^3}a_1^{(2)}, \tag{13}$$

where $Z_b = \sqrt{\mu/\varepsilon}$ is the wave impedance in the background medium.

Note that, for a pair of chiral particles, the fields $\mathbf{E}$ and $\mathbf{H}$ hitting on each particle should include the initial incident fields and the scatted fields from the other particle. Based on the coupled-dipole approximation [52,53], the total electromagnetic fields received by each particle can be computed by

$$\begin{aligned}
\mathbf{E}_o &= \mathbf{E}_{\mathrm{inc},o} + \overleftrightarrow{\mathbf{G}}_e(\mathbf{d})\mathbf{p}_d + \frac{1}{c}\mathbf{G}_m(-\mathbf{d})\mathbf{m}_d,\\
\mathbf{H}_o &= \mathbf{H}_{\mathrm{inc},o} + \frac{1}{Z_b}\left[-\mathbf{G}_m(-\mathbf{d})\mathbf{p}_2 + \frac{1}{c}\mathbf{G}_e(\mathbf{d})\mathbf{m}_d\right],\\
\mathbf{E}_d &= \mathbf{E}_{\mathrm{inc},d} + \overleftrightarrow{\mathbf{G}}_e(\mathbf{d})\mathbf{p}_o + \frac{1}{c}\mathbf{G}_m(\mathbf{d})\mathbf{m}_o,\\
\mathbf{H}_d &= \mathbf{H}_{\mathrm{inc},d} + \frac{1}{Z_b}\left[-\mathbf{G}_m(\mathbf{d})\mathbf{p}_o + \frac{1}{c}\mathbf{G}_e(\mathbf{d})\mathbf{m}_o\right],
\end{aligned} \tag{14}$$

with

$$\begin{aligned}
\mathbf{p}_o &= \alpha_{ee,o}\mathbf{E}_o + \alpha_{em,o}\mu\mathbf{H}_o,\\
\mathbf{m}_o &= -\alpha_{em,o}\mathbf{E}_o + \alpha_{mm,o}\mu\mathbf{H}_o,\\
\mathbf{p}_d &= \alpha_{ee,d}\mathbf{E}_d + \alpha_{em,d}\mu\mathbf{H}_d,\\
\mathbf{m}_d &= -\alpha_{em,d}\mathbf{E}_d + \alpha_{mm,d}\mu\mathbf{H}_d,
\end{aligned} \tag{15}$$

where the subscript o and d for all quantities in Eqs. (14) and (15) correspond to two particles located at the origin and $x = d$, and

$$\overleftrightarrow{\mathbf{G}}_e(\mathbf{d}) = \frac{e^{ikd}}{4\pi\varepsilon d^3}\left[(-k^2d^3 - 3ikd + 3)\frac{\mathbf{d}(\mathbf{d})^T}{d^2} + (k^2d^2 + ikd - 1)\overleftrightarrow{\mathbf{I}}\right]\cdot,$$

$$\mathbf{G}_m(\mathbf{d}) = \frac{ik(ikd-1)e^{ikd}}{4\pi\varepsilon d^3}\mathbf{d}\times, \tag{16}$$

are electric- and magnetic-field propagators (also called the dyadic Green's functions) [39].

Substituting Eq. (12) into Eq. (11), the force expression can be written as

$$\langle\mathbf{F}\rangle = \mathbf{F}_{\text{grad}} + \mathbf{F}_{\text{rad}} + \mathbf{F}_{\text{curl}} + \mathbf{F}_{\text{spin}} + \mathbf{F}_{\text{flow}}, \tag{17}$$

with

$$\mathbf{F}_{\text{grad}} = -\nabla\langle U\rangle,$$

$$\mathbf{F}_{\text{rad}} = \frac{1}{c}(C_{\text{ext}} + C_{\text{recoil}})\langle\mathbf{S}\rangle,$$

$$\mathbf{F}_{\text{curl}} = \nabla\times\left[C_p c\langle\mathbf{L}_s^p\rangle + C_m c\langle\mathbf{L}_s^m\rangle + \mu\text{Re}(\alpha_{em})\langle\mathbf{S}\rangle\right],$$

$$\mathbf{F}_{\text{spin}} = \left[2\omega^2\mu\text{Re}(\alpha_{em}) - \frac{k^5}{3\pi\varepsilon^2}\text{Im}(\alpha_{ee}\alpha_{em}^*)\right]\langle\mathbf{L}_s^p\rangle + \left[2\omega^2\mu\text{Re}(\alpha_{em}) - \frac{k^5\mu}{3\pi\varepsilon}\text{Im}(\alpha_{mm}\alpha_{em}^*)\right]\langle\mathbf{L}_s^m\rangle,$$

$$\mathbf{F}_{\text{flow}} = \frac{ck^4\mu^2}{12\pi}\text{Im}(\alpha_{ee}\alpha_{mm}^*)\text{Im}(\mathbf{E}\times\mathbf{H}^*),$$

where $\mathbf{F}_{\text{grad}}$ denotes the gradient force, with the optical potential energy $\langle U\rangle = -\frac{1}{4}\text{Re}(\alpha_{ee})|\mathbf{E}|^2 - \frac{1}{4}\text{Re}(\alpha_{mm})|\mathbf{B}|^2 + \frac{1}{2}\text{Im}(\alpha_{em})\text{Im}(\mathbf{B}\cdot\mathbf{E}^*)$; $\mathbf{F}_{\text{rad}}$ is the radiation force proportional to the time-averaged Poynting vector $\langle\mathbf{S}\rangle = \frac{1}{2}\text{Re}[\mathbf{E}\times\mathbf{H}^*]$; $\mathbf{F}_{\text{curl}}$ describes the curl force due to the curl of the time-averaged spin angular momentum (SAM) densities [54], with $\langle\mathbf{L}_s^p\rangle = \frac{\varepsilon}{4i\omega}\mathbf{E}\times\mathbf{E}^*$ and $\langle\mathbf{L}_s^m\rangle = \frac{\mu}{4i\omega}\mathbf{H}\times\mathbf{H}^*$; $\mathbf{F}_{\text{spin}}$ represents the spin force due to the direct coupling of particle chirality to SAM densities; and $\mathbf{F}_{\text{flow}}$ is related to the alternating flow of the "stored energy" [39]. The cross section $C_{\text{ext}} = C_p + C_m$ is a summation of the electric- and magnetic-dipole part, written as $C_p = k\text{Im}(\alpha_{ee})/\varepsilon$ and $C_m = k\mu\text{Im}(\alpha_{mm})$. The term $C_{\text{recoil}} = -\frac{k^4\mu}{6\pi\varepsilon}[\text{Re}(\alpha_{ee}\alpha_{mm}^*) + |\alpha_{em}|^2]$ is the cross section directly associated with the recoil force [47].

Next, we calculate the x and y components of each term in Eq. (17) for the different chiral cases immersed in x- and y-polarized plane waves propagating along the z axis. The results are shown in Figs. 4–6, where all the other parameters are the same as those in Fig. 1. The term $\mathbf{F}_{\text{flow}}$ in Eq. (17) has a negligible contribution to all these cases and thereby is not plotted for clarity. Also, the total forces F_x and F_y in Eq. (17) are plotted for comparison, which agrees perfectly with the results based on the FWS, corroborating the analysis within the dipole approximation. As a typical example of demonstration, Fig. 4 shows the x components of decomposed optical forces on the two particles with the chirality parameters ($\kappa_o = 0$, $\kappa_d = 0.5$), where we can see that the binding force F_x acting on either particle originates overwhelmingly from the gradient

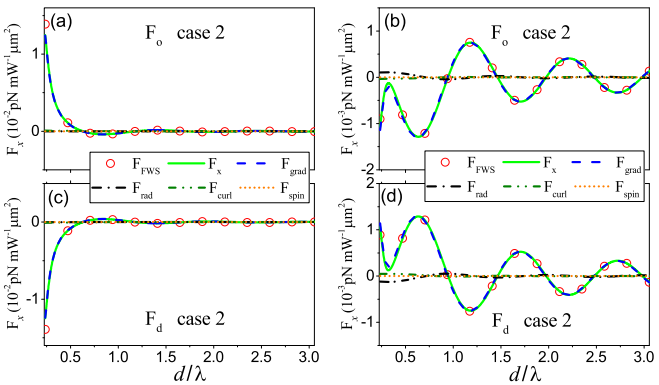

FIG. 4. The x components of decomposed optical forces on the two particles with the chirality parameters ($\kappa_o = 0$, $\kappa_d = 0.5$). The incident electric field is polarized along the (a), (c) x axis and along the (b), (d) y axis. The accurate total transverse optical force F_{FWS} based on the FWS is replotted for comparison.

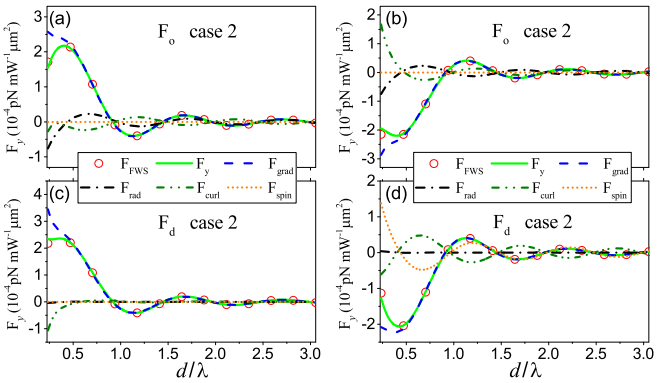

FIG. 5. The y components of decomposed optical forces on the two particles with the chirality parameters ($\kappa_o = 0$, $\kappa_d = 0.5$). The incident electric field is polarized along (a), (c) the x axis and along (b), (d) the y axis. The accurate total transverse optical force F_{FWS} based on the FWS is replotted for comparison.

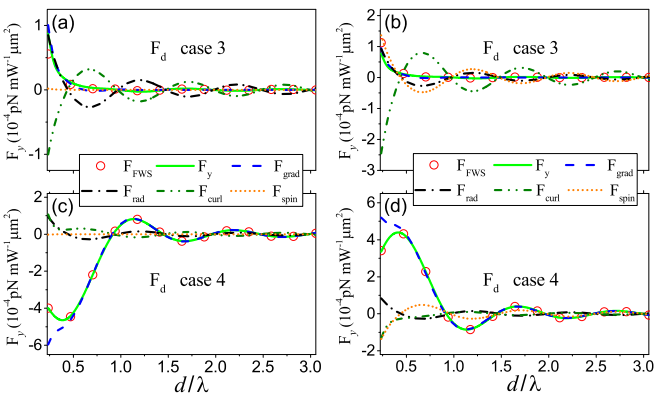

FIG. 6. The y components of decomposed optical forces on the chiral particle located at $x = d$ illuminated by a plane wave with (a), (c) x polarization and (b), (d) with y polarization. The two chiral particles have (a), (b) identical handedness ($\kappa_o = \kappa_d = 0.5$) and (c), (d) opposite handedness ($\kappa_o = -\kappa_d = 0.5$).

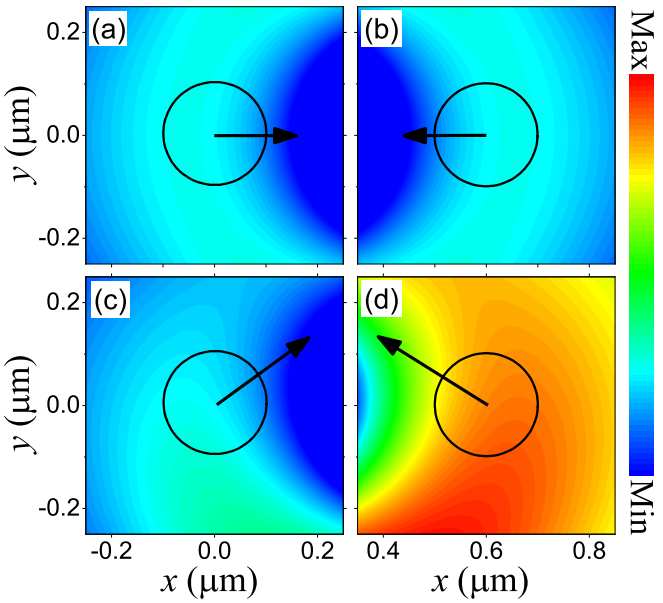

FIG. 7. Optical potential energy $\langle U \rangle$ in the proximity of the paired particles with chirality parameters (a), (b) $\kappa_o = \kappa_d = 0$ and (c), (d) $\kappa_o = 0$, $\kappa_d = 0.5$ under of the illumination by the x-polarized plane wave. The black circles and arrows denote the position and the gradient force in the $z = 0$ plane.

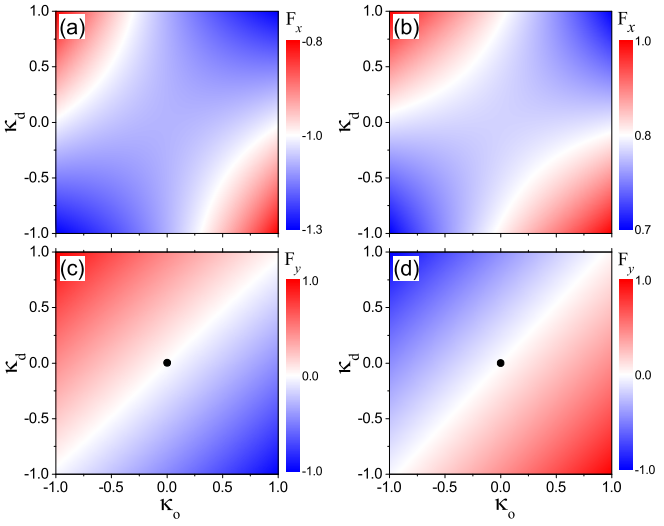

FIG. 8. The transverse optical force on the particle located at $d = 0.5$ μm versus the chirality parameters of two particles κ_o and κ_d. The other particle is positioned at the origin. (a), (b) The x component of optical force F_x. (c), (d) The y component of optical force F_y. The incident electric field is polarized along (a), (c) the x axis and along (b), (d) the y axis. The optical force is in units of 10^{-3} p N m W^{-1} μm^2. The black dots denote the vanishing of the lateral force.

force $\mathbf{F}_{\text{grad}}$. In addition, the origin of F_x on the chiral particle is the same as that of the nonchiral particle for the incident wave with the same polarization. The similar results are also found for the cases of two chiral particles with the same or opposite handedness. Differently, the lateral forces F_y on the two particles exhibit different origins as presented in Fig. 5. For the incident wave with x polarization, F_y on the nonchiral particle arises largely from the gradient force, the radiation force, and the curl force, while F_y on the chiral particle comes from the gradient force and the curl force, although their origins are both dominated by the gradient force; see Figs. 5(a) and 5(c). One can find from Figs. 5(b) and 5(d) for the incident wave with y polarization that F_y on the nonchiral particle arises from the gradient force, the radiation force, and the curl force while F_y on the chiral particle is dominated by the gradient force, the curl force, and the spin force. It is worth pointing out that the physical origins of the lateral force on the nonchiral particle in our cases both differ fundamentally from all those reported previously [19–31].

The origins of the lateral forces F_y on the two chiral particles that have the same chirality magnitude and the same or opposite handedness also examined in Fig. 6, where F_y on the particle located at $x = d$ is solely presented because the lateral force on the other particle positioned at the origin has the same physical origin. For the x-polarized plane wave, the forces F_y for the cases of two chiral particles with the same or opposite handedness both come from the gradient force, the radiation force, and the curl force, as illustrated in Figs. 6(a) and 6(c). The scenario differs distinctly from the case for the y-polarized plane wave, see Figs. 6(b) and 6(d), where the forces F_y for the above two cases are attributed to the gradient force, the radiation force, the curl force, and the spin force. It is also found that, for the case of two chiral particles with opposite handedness, the lateral force depends mainly on the gradient force for the two linear polarizations, similar to the result reported in Ref. [20].

To demonstrate intuitively the influence of the particle chirality on the transverse optical force due to the contribution from the gradient force, we plot the optical potential maps for a typical example with two particles consisting of one nonchiral particle and one chiral particle immersed in the x-polarized plane wave. In Figs. 7(c) and 7(d), the time-averaged potential energy $\langle U \rangle$ in proximity of the two particles corresponds to the cases without and with chirality, respectively. We can see that asymmetric optical potentials occur for both particles and a strong optical potential gradient along both x and y directions can be observed, giving rise to the binding force and the lateral force, consistent with the analysis within the dipole approximation. In contrast, the optical potential energy always preserves symmetry with respect to $-y$ and $+y$ for the two nonchiral particles; see Figs. 7(a) and 7(b), thus yielding a vanishing lateral force. Note that the optical potential energy always exhibits inhomogeneity along x around the particle center, leading to a nonvanishing x component of the transverse optical force that constitutes significantly to the binding force F_x.

IV. DEPENDENCE OF OPTICAL FORCE ON PARTICLE CHIRALITY

The transverse optical forces as functions of the chiral parameters of the two particles κ_o and κ_d are depicted in Fig. 8 to present the full picture of the contribution from the particle chirality, where F_x and F_y on the particle located at $d = 0.5$ μm is plotted because a similar result can also be obtained from the other particle positioned at the origin. For the binding

force F_x in the cases of two different linear polarizations, we can see from Figs. 8(a) and 8(b) that the maps of the binding forces both exhibit a nearly symmetric behavior with respect to $\kappa_o = \kappa_d$ and $\kappa_o = -\kappa_d$, less sensitive to the exchange of the two chirality parameters. In particular, with careful analysis we can find that F_x for the case with (κ_o, κ_d) is always equal to that with opposite handedness $(-\kappa_o, -\kappa_d)$, independent of the handedness. This lies in the fact the polarizabilities α_{ee} and α_{mm} associated with the Mie coefficients $a_1^{(1)}$ and $b_1^{(1)}$ are both even functions of the chirality parameter κ, as discussed in detail in Refs. [38,55]. In addition, the sign change of F_x from negative to positive in Figs. 8(a) and 8(b) indicates the transition from binding to antibinding for the paired particle, suggesting that the polarization of light can serve as an important handle in optical manipulation. Nevertheless, for the lateral force F_y, the situation is remarkably different, as illustrated in Figs. 8(c) and 8(d). By comparing Figs. 8(a) and 8(b), it can be found that a sign change appears when the polarization is switched from the x direction to the y direction. In addition, the map also exhibits an odd-function-like behavior in that $F_y(\kappa_o, \kappa_d) = -F_y(-\kappa_o, -\kappa_d)$, namely, the lateral force has the same magnitude but opposite sign with the opposite handedness $(-\kappa_o, -\kappa_d)$. Thus, the lateral force depends strongly on the magnitude and the handedness of the particle chirality for the reason that the polarizability α_{em} related to the Mie coefficient $a_1^{(2)}$ is an odd function of κ, as also discussed in Refs. [38,55]. By examining the numerical results, it is concluded that the lateral force has a very small magnitude when κ_o is close to κ_d and vanishes when the two particles are nonchiral simultaneously, as denoted by the black dots in the Figs. 8(c) and 8(d). These interesting results are in accordance with the discussions in the second part.

V. CONCLUSION

In summary, we have investigated the OB and the lateral forces of two particles with different chirality parameters immersed in a plane wave with its electric field parallel and perpendicular to the pair axis. By using the FWS based on multiple-scattering theory and generalized Lorenz-Mie theory, we have calculated the transverse force, namely, the binding force and the lateral force, on each particle versus the interparticle separation. For the incident plane wave with the two different linear polarizations, the binding forces along the pair axis for the chiral case show a similar behavior for the nonchiral case and are much less sensitive to the magnitude and handedness of the particle chirality. In particular, there are multiple stable dimer states appearing at different particle distances for different linear polarizations, and the binding forces decrease with increasing particle separation. However, the lateral force, perpendicular to the pair axis and the light propagation, depends strongly on the magnitude and handedness of the particle chirality. The analytical results within the dipole approximation reveal that the binding force depends largely on the gradient force while the lateral force arises from the gradient force, radiation force, curl force, and spin force due to the interparticle interaction mediated by the light.

ACKNOWLEDGMENTS

This work was supported by the National Natural Science Foundation of China (Grants No. 11804061, No. 11574275, and No. 11574055), the Natural Science Foundation of Guangxi Province (Grant No. 2018GXNSFBA281021), the Zhejiang Provincial Natural Science Foundation of China (Grant No. LR16A040001), the Scientific Base and Talent Special Project of Guangxi Province (Grant No. AD19110095), the Open Project of State Key Laboratory of Surface Physics in Fudan University (Grant No. KF2019_11), the Research Program of Science for Universities of Guangxi Province (Grant No. 2018KY0328), and the Innovation Project of GuangXi University of Science and Technology Graduate Education (Grant No. GKYC201905).

[1] M. M. Burns, J. M. Fournier, and J. A. Golovchenko, Phys. Rev. Lett. **63**, 1233 (1989).
[2] M. M. Burns, J. M. Fournier, and J. A. Golovchenko, Science **249**, 749 (1990).
[3] D. Bradshaw, K. Forbes, J. Leeder, and D. Andrews, Photonics **2**, 483 (2015).
[4] S. K. Mohanty, J. T. Andrews, and P. K. Gupta, Opt. Express **12**, 2746 (2004).
[5] J. Ng, Z. F. Lin, C. T. Chan, and P. Sheng, Phys. Rev. B **72**, 085130 (2005).
[6] V. Demergis and E. Florin, Nano Lett. **12**, 1 (2012).
[7] P. C. Chaumet and A. Rahmani, Phys. Rev. B **87**, 195125 (2013).
[8] M. T. Wei, J. Ng, C. T. Chan, and H. D. Ou-Yang, Sci. Rep. **6**, 1 (2016).
[9] Y. Arita, E. M. Wright, and K. Dholakia, Optica **5**, 910 (2018).
[10] K. Dholakia and P. Zemanek, Rev. Mod. Phys. **82**, 1767 (2010).
[11] T. Čižmár, L. C. Dávila Romero, K. Dholakia, and D. L. Andrews, J. Phys. B: At., Mol. Opt. Phys. **43**, 102001 (2010).
[12] R. W. Bowman and M. J. Padgett, Rep. Prog. Phys. **76**, 026401 (2013).
[13] K. A. Forbes and D. L. Andrews, Phys. Rev. A **91**, 053824 (2015).
[14] Y. Zhu, Z. Wua, Z. Lia, and Q. Shanga, Procedia Eng. **102**, 329 (2015).
[15] V. Karásek, T. Čižmár, O. Brzobohatý, P. Zemánek, V. Garcés-Chávez, and K. Dholakia, Phys. Rev. Lett. **101**, 143601 (2008).
[16] V. Karásek, O. Brzobohatý, and P. Zemánek, J. Opt. A **11**, 034009 (2009).
[17] J. Bai, Z. S. Wu, C. X. Ge, Z. J. Li, T. Qu, and Q. C. Shang, J. Quant. Spectrosc. Radiat. Transfer **214**, 71 (2018).
[18] G. A. Swartzlander, Jr., T. J. Peterson, A. B. Artusio-Glimpse, and A. D. Raisanen, Nat. Photonics **5**, 48 (2011).
[19] S. B. Wang and C. T. Chan, Nat. Commun. **5**, 3307 (2014).
[20] H. J. Chen, Y. K. Jiang, N. Wang, W. L. Lu, S. Y. Liu, and Z. F. Lin, Opt. Lett. **40**, 5530 (2015).
[21] K. Y. Bliokh, A. Y. Bekshaev, and F. Nori, Nat. Commun. **5**, 3300 (2014).

[22] A. Hayat, J. P. B. Mueller, and F. Capasso, Proc. Natl. Acad. Sci. USA **112**, 13190 (2015).
[23] M. Antognozzi, C. R. Bermingham, R. L. Harniman, S. Simpson, J. Senior, R. Hayward, H. Hoerber, M. R. Dennis, A. Y. Bekshaev, K. Y. Bliokh, and F. Nori, Nat. Phys. **12**, 731 (2016).
[24] F. J. Rodríguez-Fortuño, N. Engheta, A. Martínez, and A. V. Zayats, Nat. Commun. **6**, 8799 (2015).
[25] S. Sukhov, V. Kajorndejnukul, R. R. Naraghi, and A. Dogariu, Nat. Photonics **9**, 809 (2015).
[26] H. J. Chen, C. H. Liang, S. Y. Liu, and Z. F. Lin, Phys. Rev. A **93**, 053833 (2016).
[27] A. Y. Bekshaev, K. Y. Bliokh, and F. Nori, Phys. Rev. X **5**, 011039 (2015).
[28] T. Zhang, M. C. Mahdy, Y. Liu, J. H. Teng, C. T. Lim, Z. Wang, and C. Qiu, ACS Nano **11**, 4292 (2017).
[29] H. Chen, Q. Ye, Y. Zhang, L. Shi, S. Liu, Z. Jian, and Z. Lin, Phys. Rev. A **96**, 023809 (2017).
[30] V. Svak, O. Brzobohatý, M. Šiler, P. Jákl, J. Kaňka, P. Zemánek, and S. H. Simpson, Nat. Commun. **9**, 5453 (2018).
[31] H. Magallanes and E. Brasselet, Nat. Photonics **12**, 461 (2018).
[32] M. M. Li, S. H. Yan, Y. N. Zhang, Y. S. Liang, P. Zhang, and B. L. Yao, Phys. Rev. A **99**, 033825 (2019).
[33] C. F. Bohren and D. R. Huffman, *Absorption and Scattering of Light by Small Particles* (John Wiley and Sons, New York, 1983).
[34] J. A. Kong, *Electromagnetic Wave Theory* (John Wiley and Sons, New York, 1990).
[35] I. V. Lindell, A. H. Sihvola, S. A. Tretyakov, and A. J. Viitanen, *Electromagnetic Waves in Chiral and Bi-Isotropic Media* (Artech House, Boston, 1994).
[36] Y. L. Xu, Appl. Opt. **34**, 4573 (1995).
[37] G. Gouesbet and G. Grehan, *Generalized Lorenz-Mie Theories* (Springer, Berlin, 2011).
[38] H. J. Chen, N. Wang, W. L. Lu, S. Y. Liu, and Z. F. Lin, Phys. Rev. A **90**, 043850 (2014).
[39] J. D. Jackson, *Classical Electrodynamics*, 3rd ed. (John Wiley and Sons, New York, 1999).
[40] Q. Ye and H. Z. Lin, Eur. J. Phys. **38**, 045202 (2017).
[41] J. P. Barton, D. R. Alexander, and S. A. Schaub, J. Appl. Phys. **66**, 4594 (1989).
[42] Ø Farsund and B. U. Felderhof, Physica A (Amsterdam, Neth.) **227**, 108 (1996).
[43] N. Wang, J. Chen, S. Y. Liu, and Z. F. Lin, Phys. Rev. A **87**, 063812 (2013).
[44] R. P. Cameron, S. M. Barnett, and A. M. Yao, New J. Phys. **16**, 013020 (2014).
[45] R. Cameron, A. Yao, and S. Barnett, J. Phys. Chem. A **118**, 3472 (2014).
[46] M. Nieto-Vesperinas, J. J. Sáenz, R. Gómez-Medina, and L. Chantada, Opt. Express **18**, 11428 (2010).
[47] J. Chen, J. Ng, Z. F. Lin, and C. T. Chan, Nat. Photonics **5**, 531 (2011).
[48] K. Ding, J. Ng, L. Zhou, and C. T. Chan, Phys. Rev. A **89**, 063825 (2014).
[49] Y. K. Jiang, H. J. Chen, J. Chen, J. Ng, and Z. F. Lin, arXiv:1511.08546.
[50] M. Nieto-Vesperinas, Phys. Rev. A **92**, 043843 (2015).
[51] A. Lakhtakia, V. K. Varadan, and V. V. Varadan, *Time-Harmonic Electromagnetic Fields in Chiral Media* (Springer-Verlag, Berlin, 1989).
[52] G. W. Mulholland, C. F. Bohren, and K. A. Fuller, Langmuir **10**, 2533 (1994).
[53] T. Lemaire, J. Opt. Soc. Am. A **14**, 470 (1997).
[54] C. Cohen-Tannoudji, J. Dupont-Roc, and G. Grynberg, *Photons and Atoms: Introduction to Quantum Electrodynamics* (John Wiley and Sons, New York, 1989).
[55] W. L. Lu, H. J. Chen, S. D. Guo, S. Y. Liu, and Z. F. Lin, Opt. Lett. **43**, 2086 (2018).